British Ceramic Proceedings ***59***, edited by W. Lee and B. Derby (Institute of Materials, 1999), 45-60.

Hertzian Testing of Ceramics

S.G. Roberts
Department of Materials
University of Oxford
Parks Road
Oxford
OX1 3PH, UK

Abstract

The paper reviews recent work on the fracture mechanics of ring crack formation, from pre-existing small surface cracks, when a hard sphere is pressed elastically against a hard surface. It summarises the ways in which data from these "Hertzian" tests may be used to determine the extent of surface cracking damage, the materials fracture toughness, and the strength of any residual stress in the surface. Examples are given of experiments applying these test methods.

Introduction

If a hard sphere is pressed against a hard surface, the contact is purely elastic at low and moderate loads. If the load on the indenter is P and the indenter radius is R then the radius of the contact area, a, is given by[1,2]:

$$a = \left(3RP/4E^*\right)^{1/3} \tag{1}$$

where

$$1/E^* = \left(1-\nu_1^2\right)/E_1 + \left(1-\nu_2^2\right)/E_2 \tag{2}$$

ν_1, ν_2 and E_1, E_2 are Poisson's ratio and Young's modulus for the sphere and substrate respectively. The peak pressure under the contact is p_o:

$$p_o = 3P/2\pi a^2 = (3/2\pi)(P)^{1/3}\left(4E^*/3R\right)^{2/3} \tag{3}$$

The resulting stress field in the test specimen, though complex, has been completely characterised [1,2]. The principal feature, from the point of view of fracture mechanics, is a radial stress that is tensile close to the surface. This tensile stress decays with distance, r, from the contact centre:

$$\sigma_{rr} = \frac{1-2\nu}{2}\frac{P}{\pi r^2} \qquad (4)$$

The radial stress decreases rapidly with depth and eventually becomes compressive (see Figure 1). At sufficiently high indenting loads, the near-surface radial tensile stress can propagate a pre-existing crack in the surface. The initial stage of propagation is to form a ring around the contact centre. Subsequent increases in loading may then stably drive the ring deeper; the crack follows the principal tensile stress trajectory, to form a characteristic "cone crack"; the mechanics of this stage are outside the scope of this paper.

This paper reviews recent work on the fracture mechanics of ring crack formation in brittle materials, and summarises the ways in which data from Hertzian tests may be used to determine the extent of surface cracking damage, the material's fracture toughness, and the strength of any residual stress in the surface. Examples are given of experiments applying these test methods.

Surface Flaw Testing

The test method for the determination of the populations of surface-breaking cracks in brittle materials using Hertzian indentation is to perform a number of tests on the surface, to the point at which a ring crack is formed in each test. (In our test instrument, the formation of ring cracks is detected by the associated acoustic emission.) For each test, one then measures the diameter of the ring crack. It is then possible, from the ring crack diameter and the ring crack formation load, to determine the size of the surface flaw that was the origin of the ring crack. To do this, it is necessary to find the size of the crack at the radial position of the ring that, at the fracture load, experiences a stress intensity equal to the critical stress intensity for fracture, K_{Ic}.

British Ceramic Proceedings ***59***, edited by W. Lee and B. Derby (Institute of Materials, 1999), 45-60.

There have been a number of papers calculating the stress intensity factors associated with cracks driven by Hertzian indentation [2-7]. Early calculations of this type used only the near-surface radial tensile stress component of the stress field, effectively assuming that this stress was uniformly applied to the crack. However, the stress field actually decays rapidly with increasing depth, and most of the crack surfaces are subjected to a lower tensile traction than that resulting from the near-surface stress (see Figure 1). If the crack is deep enough, the stress on some parts of the crack faces may even be compressive.

Cracks will thus experience a stress intensity lower than that calculated assuming that they are in a uniform stress equal to the surface radial stress. Recently, Warren et al. [8] applied the distributed dislocation technique [9] to Hertzian fracture. This method allows efficient evaluation of the stress intensity factors in strongly varying stress fields. We have used these stress intensity calculations in the interpretation of the experimental data and in the simulation of Hertzian testing described in this paper.

The stress intensity factors used in this paper are calculated for the relatively simple case of a planar crack of depth c, normal to and intersecting the free surface. This an approximation to the real situation. The cracks are likely to be "thumbnail" cracks of a length comparable to their depth, though on a scratched or abraded surface such cracks may lie in closely connected or overlapping "chains", thus resembling planar cracks. Two questions then arise: (1) what type of crack, linear or thumbnail, should one use to calculate stress intensity factors); (2) if a thumbnail crack, what aspect ratio should be used, and where on the crack front should K be calculated. A detailed analysis by Lin et al[10] has compared the stress intensity factors associated with elliptical thumbnail cracks, of various aspect ratios, in the Hertzian stress field with those associated with planar cracks. They found that for all thumbnail cracks, while the stress intensity at the deepest point of the cracks is rather less than for a planar crack of the same depth, the stress intensity factor near the free surface was always very close to that of a planar crack of the same depth, and with 2% of the planar crack value for all elliptical cracks wider than their depth. Thus the assumed stages of crack propagation for a thumbnail crack are (1) K exceeds K_{Ic} only near the surface of the crack - it extends rapidly "sideways" to form a ring crack (2) K now exceeds K_{Ic} at the base of the ring crack, and this may

extend rapidly in depth until K at the base of the crack drops below K_{Ic}. In practice these stages may be near-simultaneous. Swindlehurst and Lawn[11] could not distinguish these two stages in their acoustic emission studies of ring crack formation. Whatever the initial crack shape, however, the study of Lin et al indicates that the stress intensity calculations outlined below do give the conditions for unstable crack extension to occur, eventually forming the ring system.

Flaw sizes and Flaw densities

In a given test, a ring crack forms at indentation load (P); the radius of the ring crack generated (r) gives the distance of the originating flaw from the contact centre. The depth of the original (surface-breaking) flaw (c) is calculated by finding the depth of the crack at position r which has $K = K_{Ic}$ at load P. For surfaces with other than very sparse flaw distributions, use of the following approximate expression[8] for K as a function of P, c and r gives results very close to those using the full calculation:

$$K_I = 1.12\, p_0 \sqrt{\pi a} \sqrt{\frac{c}{a}} \left(\frac{(1-2\nu)}{3\left(\frac{r}{a}\right)^2} - \frac{2\alpha\left(\frac{c}{a}\right)}{\pi} \right), \qquad (5)$$

where a and p_0 are calculated as in equations 1 and 3, and α is given by:

$$\alpha = \frac{-1}{\sqrt{u}} \left[u\left(\frac{1-\nu}{1+u}\right) - 2(1+\nu)\sqrt{u}\, \tan^{-1}\left(\frac{1}{\sqrt{u}}\right) \right] \qquad (6)$$

with:

$$u = \left(\frac{r}{a}\right)^2 - 1 \qquad (7)$$

Thus, each test gives a value of r (the ring crack radius) and P (the indenting load to produce the ring crack). Equations 1 -3 are then used to calculate a and p_0 for each test, then either the full numerical solution for K as a function of crack size and position, or the approximate solution above, is used iteratively to find the value of crack depth for which $K = K_{Ic}$. This is taken as the size of the original flaw. The simplest way to present data derived from a series of tests is to examine the distribution of flaws found within a given size range. Figure 2 shows the results of such tests on two alumina samples, identical apart

from their surface finish. The mean flaw depth for the "abraded" surface (ground with 600 grit SiC) was 6.4μm, and that for the "polished" surface (ground and then finished with 6μm diamond paste) was 4.6μm; the figure shows the increased spread in flaw size produced by the grinding treatment.

A more sophisticated treatment of the data is to calculate the density of flaws found in the surfaces; i.e. the number per unit area of flaws in a given size range. This is done by invoking the concept of "searched area", originally proposed and used by Wilshaw [2]. The searched area for cracks within a given size range is evaluated as follows: for each test, calculate the area of the test surface around the indentation within which, had there been a crack of a size within the range of interest, it would have formed a ring crack at a load below that actually reached during the test (usually the calculation is done for a crack of a size midway in the range). These searched areas are annuli surrounding each test site, the inner and outer radii of which vary with the depth of the crack being "searched" for. Then, in a series of tests, the total searched area for cracks within a given size range is simply the sum of all the searched areas for individual tests. The crack density, $\rho(c)$ (cracks per unit area of test surface) is then calculated as:

$$\rho(c_1 < c < c_2) = \frac{\text{Number of crack found}(c_1 < c < c_2)}{\text{Total searched area}\ (c = (c_1 + c_2)/2)} \qquad (8)$$

Some complications in the calculation of searched areas were not taken into account in Wilshaw's use of the method [2]; the equations given effectively assume that (a) all cracks are oriented circumferentially with respect to the indentation centre; (b) the stress acting on each crack is the surface skin stress. Both of these factors overestimate the stress intensity acting on an "average" flaw, and thus overestimate the searched areas.

The first effect leads to a very large error in the searched area and calculated crack densities, as only a very small fraction of the cracks present in a randomly damaged surface will have orientations close to the circumferential direction; cracks even a few degrees from this orientation will have very substantially lower stress intensities acting on them, and will be effectively "invisible" to the Hertzian test. The second effect becomes more important as deeper cracks are considered, and can lead to the inner radius of the searched

area varying its position in a complicated way with increasing load, making the calculations of searched area more complex. However, all these effects can be taken into account [12] and we have developed computer codes to calculate real searched areas and thus crack densities (these are two or three orders of magnitude higher than those calculated using Wilshaw's original searched area equations [2]).

Figure 3b shows the crack densities calculated using this extension of Wilshaw's method for the tests shown as "number of cracks found" in Figure 3a. The data are from tests done on alumina / SiC "nanocomposite" ceramics [13] and show the improved surface finish produced in the nanocomposite for the same polishing treatment.

Clearly, a certain minimum number of tests need to be done to find a representative number of the cracks actually present in a given surface; to get any data on the rarer cracks, enough tests need to be done to find at least one, preferably more. To see how many tests need to be done to gain a reasonably accurate picture of the true flaw densities, we performed computer simulations of Hertzian testing

Simulated Tests

The method used was to generate a distribution of flaws random in position and orientation, corresponding to operator-defined flaw densities for each crack size, around a point at which a simulated test was performed. The test steadily increases the simulated load until the first flaw with $K = K_{Ic}$ is found, and the size, position and orientation of the critical flaw noted. Each "test" in a series is performed in a newly-randomised flaw distribution.

Data from simulated tests on different types of flaw distribution are shown in Figure 4 (test surface and test ball of alumina, 10mm diameter ball). The flaw distributions used as input data are shown in Figure 4a; we used:

1. Two "flat" flaw distributions, F1 and F2, with an equal density for all flaw sizes – while probably rather unrealistic, this should provided a simple base for comparison with more realistic distributions;
2. Three "decreasing" flaw distributions, D1, D2 and D3, where the flaw density is lower for longer cracks; this probably corresponds to the state of a well –polished surface;
3. One "peaked" flaw distribution, DP, where the flaw density is a maximum at a given flaw size; this type of distribution might correspond to that in a surface abraded with a particular grit size.

Results are shown in Figure 4b, as cumulative probability of (ring) fracture as a function of test load. This type of plot is used in experiments as a simple "first view" of the data, before the rather lengthy ring crack size measurements and subsequent calculations to give flaw densities are done, and is was of interest to see what type of information could be extracted from such plots alone.

The plots have two main features of interest:

1. There is a definite minimum load for fracture, which does not vary significantly with the details of the flaw distribution. The reasons for this, and its uses to calculate K_{Ic} and residual stresses, are outlined later in this paper.
2. The slope of the plots is closely related to the flaw density around ~10μm flaw size; "flat", "decreasing" and "peaked" flaw distributions with high flaw density at this flaw size (F1, D1, DP) all have steeply rising fracture probability / load graphs. All flaw distributions with low flaw densities at this flaw size have more slowly rising, and scattered, fracture probability / load graphs.

This tendency for tests to "focus" on flaws in a narrow size range is shown in Figure 5. The flaw distribution deduced from the test results is peaked around a favoured flaw size, which increases with increasing test ball size. It is possible for cracks, even if present in large numbers, not to be detected at all if they are of a size very different from the favoured one for the size of ball used. The reasons for this are explored below.

Minimum Fracture Load

The reasons for the existence of the minimum fracture load shown in Figure 4 and in all experimental results from Hertzian tests are connected with the decrease in radial stress with depth and radial position illustrated in Figure 1; this was first noted by Warren [14]. At any given load, the complexity of the stress field around the contact means that there is one position and depth of surface-breaking crack for which the crack has the maximum possible stress intensity. This crack is indicated by a heavy line in Figure 1. Cracks deeper than this have tips that find themselves in a decreasing or even compressive parts of the stress field, cracks closer to the contact centre again have crack tips in weaker or compressive parts of the stress fields, shorter cracks have lower stress intensity because of the shorter crack surface over which tensile tractions can act, and cracks further away from the contact centre are in a weaker tensile stress overall.

For a given test material / ball combination, the crack with the maximum stress intensity factor is found at a constant c/a and r/a value (that is, the absolute depth and position of this flaw increase with increasing load); the stress intensity factor on this crack increases monotonically with increasing applied load. The minimum fracture load corresponds to the load at which this "most favoured" flaw first has $K = K_{Ic}$. Below this load, there are no surface-breaking cracks, of any depth or position, that have $K \geq K_{Ic}$; ring crack formation is not possible at such loads.

The r/a value at which the "most favoured" flaw is found is typically between 1.05 and 1.2. This is as observed experimentally [4]. Previous explanations have been in terms of the statistical distribution of flaws on the test surface 4 or the effects of interfacial friction [15]; such explanations are unnecessary, as the fracture mechanics of surface breaking cracks in the full Hertzian stress field, as outlined here, give this result.

Fracture Toughness from Hertzian Testing

The minimum fracture load in Hertzian testing depends only on the elastic properties of the test ball and substrate and the fracture toughness of the test materials. If the ball and test material have different elastic

constants, then interfacial friction between the two will also influence the minimum fracture load; however we will consider here only the case where the ball and test material are identical, when frictional effects play no part. In this case, relation between K_{Ic} and the minimum load for fracture, P*, is given by [14]:

$$K_{Ic} = \left(\frac{E * P *}{C R} \right)^{1/2}, \qquad (9)$$

where the constant C depends only on the Poisson's ratio of the test material and test ball (as listed in Table 1), and R is the radius of the test ball. Thus, to determine fracture toughness, all that is required is to establish a well-defined value for the minimum load to create a Hertzian ring crack. In practice, we find that between 20 and 40 tests are usually sufficient. Plots of fracture probability against test load help to indicate whether the minimum load is well defined; a steeply rising curve above the minimum fracture load gives one confidence that a reliable value has been measured. Clearly, the method depends on there being a high probability in a series of tests that a flaw of the right depth and position will be found, in at least one test, so as to give fracture at or very close to the minimum fracture load. To this end, it is found experimentally to be useful to abrade the test surface lightly so as to introduce a moderately high flaw density. Since the constant C is very sensitive to ν, accurate determination of ν is necessary for best interpretation of data; use of a natural vibration frequency measuring instrument such a "Grindosonic" is recommended.

The method has an advantage over techniques based on sharp indentation, (e.g. that of Anstis et al. [16]), as the contact is purely elastic at all times, giving rise to a fully characterised stress field in which the small flaws in the surface can propagate. For techniques based on sharp indentation, in contrast, the final length of the median/radial cracks used to determine fracture toughness is determined by the complex elastic/plastic stress field around these indentations, which is not very well characterised; the review by Ponton and Rawlings [17] gives 19 different formulae for determining factor toughness from such experiments, which give a wide variation in the calculated results from a given set of data [18].

The detailed analysis [14] leading to equation (9) also provides the basis for "Auerbach's law" [19] that, in Hertzian fracture, the fracture load is proportional to the indenting ball radius. For tests on surfaces with a moderate or high flaw density, ring crack formation is likely to occur near to the minimum load, P*, which is proportional to the ball radius, R. Further, since in ideally brittle materials:

$$K_{Ic} = (2\gamma E)^{1/2}, \qquad (10)$$

the constant of proportionality between P* and R is linearly dependent on γ, the surface energy of the specimen material, as noted by Lawn [20].

Fracture Toughness Results

Figure 6 shows a typical experimental curve of fracture probability as a function of load for tests on glass. Note that there is a well defined minimum load for fracture, from which one can determine a value for fracture toughness. Table 2 gives values for fracture toughness determined in this way [14] for float glass and polycrystalline alumina. The mean values and standard deviations are: glass, 0.78 ± 0.08 MPam$^{1/2}$; alumina, 3.96 ± 0.27 MPam$^{1/2}$. These values are in good agreement with those in the literature - for example Zeng et. al. [7] found values of 0.8 MPam$^{1/2}$ for glass and 3.77 MPam$^{1/2}$ for alumina.

Effect of Surface Stresses

The above treatment for the determination of fracture toughness assumes that the surface is initially stress-free. A residual stress in the surface will change the stress intensity experienced by surface flaws and thus change the minimum load for Hertzian fracture [21]. Stress intensities on cracks normal to the surface were calculated as:

$$K = K_{Hertz} + K_{\sigma} \ , \qquad (11)$$

where K_{Hertz} is the stress intensity induced on the crack by the load applied to the indenting ball and K_{σ} is the stress intensity induced on the crack by the residual stress in the surface. K_{Hertz} was computed numerically using the full Hertzian stress field [8], and K_{σ} was taken as:

$$K_\sigma = 1.12\ \sigma\ (\pi c)^{1/2}\ , \qquad (12)$$

where c is the depth of the crack and σ is the surface stress, assumed to be biaxial and uniform with depth over a depth somewhat greater than that of the crack. A computer program was used to search for the crack with maximum K (K_{max}) for increasing values of indenting load P. The minimum fracture loads, P_σ^*, which gave $K_{max} = K_{Ic}$ at were noted for a range of values of σ.

Figure 7 shows the predicted effects of compressive residual stresses on the Hertzian indentation of float glass (E = 70 GPa, ν = 0.25) with a 10mm diameter ball of the same material. Figure 7a shows the maximum K on cracks normal to the surface for a given indenting load, P; Figure 7b shows the minimum fracture load (p_σ^*) as a function of residual stress (σ).

As the compressive surface stress increases in magnitude, the maximu m K possible on any surface crack reaches K_{Ic} (taken as 0.80 $MPam^{1/2}$) at loads increasingly greater than for the stress-free case. The shift in minimum fracture load in Hertzian testing can be therefore be used to determine residual stresses, provided that a sample known to be stress-free is available as a reference, or if the test material's K_{Ic} is known. (For other materials than glass, similar curves to those in Figure 7 can easily be generated.)

Approximate determination of surface residual stress

A rough estimate of the residual stress can be obtained by a knowledge of the flaw size giving fracture at the minimum load, c*. We can calculate the *apparent* fracture toughness ($^\sigma K_{Ic}$) from P_σ^* for the stressed surface according to equation (9) above; the difference from the true K_{Ic} ($^0K_{Ic}$) is then approximately:

$$^0K_{Ic} - {}^\sigma K_{Ic} = 1.12\sigma\sqrt{\pi c_0^*} \qquad (13)$$

where c_0* is the crack depth for fracture at the minimum Hertzian indentation load in a stress-free surface; (for a sphere of diameter 10mm, c_0* = 13.2 µm for glass, and 11.2 µm for alumina). Calculations of the

residual stress using c_0* give better estimates of the residual stress than those using c_σ*, the actual critical crack size and position in the stressed surface [21]. In simulated tests on stressed surfaces, results using this approximate method are within 20% of the input stress value, and often within a few %.

Residual Stress – Results

Strengthened Glass

We used the Hertzian method to obtain values for the residual stresses in the surface of chemically strengthened glass specimens. The strengthening process consists of immersing the glass specimens in a potassium nitrate bath heated to 460°C for 42 hours [22]. Potassium ions are exchanged on a one for one basis with sodium ions near the surface, with the concentration of potassium ions falling off with depth. The potassium ions are larger than the sodium ions they replace, and so a compressive stress is generated in the surface layer of the glass. For the specimens tested here, the compressive stress profile has been determined by differential surface refractometry [23]; the surface compressive stress is approximately 450 MPa, and falls off steadily with depth; at 10 μm below the surface the stress is ~380 MPa. Below a depth of approximately 40 μm virtually no ion exchange has occurred.

Figure 8 shows typical cumulative fracture probability plots versus fracture load for annealed glass (abraded with 1000 grit SiC) and chemically strengthened glass, indented with a stainless steel sphere of diameter 5mm. Because of the compressive residual stress, the minimum load for fracture for the strengthened glass, 800N, is considerably larger than that for the annealed glass, 89N.

The threshold loads were measured [21] using a variety of sphere materials (ferritic and stainless steels, WC-Co) and sphere sizes. The “apparent fracture toughness” method was used to determine residual stresses in the chemically strengthened glass specimens; apparent fracture toughnesses were within the range 1.8-2.2 MPam$^{1/2}$. The residual stress values were calculated taking the fracture toughness values for

the un-strengthened glass as 0.80 MPa $m^{1/2}$. The derived values of residual compressive stress in the chemically strengthened glass are in the range 180-240 MPa. The discrepancy between these values and the ~400 MPa determined by optical methods over the depths of the cracks may be because of modification of the elastic properties of the glass by the ion exchange process: very small changes in ν produce substantial changes in C (see Table 1). Interfacial friction between the elastically dissimilar test ball and test surface may also affect the results. Because of these possible errors, and also because of the largely unknown variation in stress with depth, the results should be regarded as "estimates" rather than as accurate determinations.

Post-grinding stresses in alumina-SiC "nanocomposites"

Most workers who have fabricated nanocomposites with Al_2O_3 grain size in the region of 2 - 4 μm with an incorporation of 5 - 10% by volume SiC of 100 - 300 nm particle size achieve bend strengths of about 800 MPa [24 - 28] compared to 350 - 400 MPa for polycrystalline alumina of the same grain size. These high strengths cannot be explained by a simple increase in toughness over the polycrystalline alumina; most workers have found only a modest increase in fracture toughness, from about 3 $MPam^{1/2}$ for a similar grain size polycrystalline alumina to about 3.5 $MPam^{1/2}$ for the nanocomposites [25,27,28].

Figure 9a shows the Hertzian indentation fracture loads from ground or polished Al_2O_3/SiC nanocomposite and polycrystalline alumina surfaces. The minimum cracking loads measured for the polished alumina and nanocomposite specimens are results from a low surface residual stress state, and show the intrinsic fracture toughnesses of the alumina and the nanocomposite to be very similar, consistent with earlier work [25-28]. The minimum Hertzian fracture loads, P*, for the as-ground surfaces are higher than for the polished surfaces for both the nanocomposite and alumina. We interpret this as the result of compressive stresses of near the surface after grinding, of ~580 MPa for the nanocomposite and about ~150 MPa for the alumina (these will be "weighted average" values over the depth of the cracks, ~10μm). Such compressive stresses provide a significant contribution to the observed high four-point bend strengths of ground nanocomposites (e.g. [24, 29]).

When the ground surfaces of the nanocomposite are annealed at 1250ºC for from 0.5 to 10 hours, the minimum fracture loads converge to ~ 500 N (Figure 9b); this is only slightly higher than the minimum fracture load for the polished surface, and corresponds to a surface compressive residual stress of ~100 MPa. Thus the majority of the surface residual stress induced by machining is rapidly removed on annealing. In an earlier paper Hertzian indentation results were interpreted as showing a significant increase in nanocomposite toughness [13]; we now believe this conclusion to be incorrect in view of the reduction in minimum fracture load of the composite on annealing. It is interesting to note that the annealing of the nanocomposites results in an increase in bend strength [24] even though the compressive residual stress drops; the reasons for this appear to be connected with surface crack healing [29].

Summary

Results from Hertzian fracture tests may be used to determine a wide variety of information about the surface state and mechanical properties of brittle materials. The data of interest are (a) the load initiating extension of a pre-existing surface-breaking crack, and (b) the diameter of the resulting “ring crack”. These data can be used as follows:

1. Ring crack size and fracture load in a given test may be used to calculate the precursor flaw depth; data from a series of tests may be used to calculate densities of flaws in a given size range.
2. Fracture load / probability curves may be used to gain a rough impression of flaw density distributions.
3. In a series of tests using a given test ball size, results tend to “focus” on particular flaw sizes; these flaw sizes are close to that for fracture at the minimum possible fracture load for the test configuration.
4. The minimum fracture load is a result of the complex elastic stress field around a Hertzian contact; it may be used in stress-free surfaces to determine fracture toughness.
5. Surface residual stresses cause shifts in the minimum load for fracture, and such shifts can be used to estimate the strength of the residual stresses and changes in residual stress with annealing, etc.

Work is continuing in developing these test methods and their applications.

British Ceramic Proceedings ***59***, edited by W. Lee and B. Derby (Institute of Materials, 1999), 45-60.

Acknowledgements:

My thanks to P.D. Warren and D.A. Hills for their contributions to the theoretical aspects covered in this paper, to C.W. Lawrence, Y. Bisrat, C.C. Anya and H-Z. Wu, for provision of experimental results, to B. Derby for discussions of the nanocomposite work and to J. Bradshaw of Pilkingtons for provision of glass specimens. The research was funded in part by the European Commission, the EPSRC and the DTI; financial support was provided by Merton College, Oxford, for Y. Bisrat and the British Council for H-Z Wu. The referees are thanked for their useful and constructive comments. Thanks also to Engineering Systems (Nottingham) for their help in developing the test instrument.

British Ceramic Proceedings ***59***, edited by W. Lee and B. Derby (Institute of Materials, 1999), 45-60.

Tables

Table 1: C (equation 9) as a function of ν (data calculated using a full numerical solution[14])

n	**C**	n	**C**
0.10	789	0.23	2490
0.11	850	0.24	2790
0.12	917	0.25	3131
0.13	991	0.26	3530
0.14	1074	0.27	4001
0.15	1167	0.28	4560
0.16	1270	0.29	5229
0.17	1386	0.30	6037
0.18	1517	0.31	7022
0.19	1665	0.32	8235
0.20	1883	0.33	9748
0.21	2025	0.34	11658
0.22	2247	0.35	14106

Table 2: Fracture toughness of glass and alumina determined by Hertzian testing.

Material	**Surface treatment**	**Sphere radius (mm)**	**Minimum fracture load (N)**	**K_{Ic} ($MPam^{1/2}$)**
Glass	As-received	2.5	127	0.78
		5.0	340	0.90
	SiC grit	2.5	105	0.71
		5.0	231	0.74
Alumina	SiC grit	2.5	470	3.72
		5.0	982	3.80
	Diamond	2.5	540	3.99
		5.0	1273	4.33

British Ceramic Proceedings ***59***, edited by W. Lee and B. Derby (Institute of Materials, 1999), 45-60.

Figures

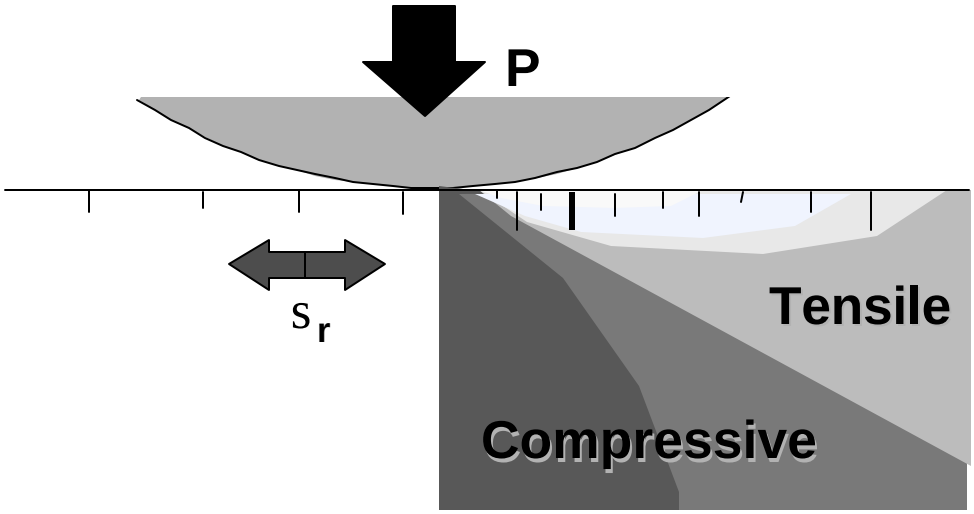

Figure 1: Radial tensile / compressive stresses around a Hertzian contact. There is a shallow region of strong tensile radial stress near the contact edge, which decreases rapidly with depth and eventually become compressive. Surface breaking cracks are generally with a strongly varying stress field.

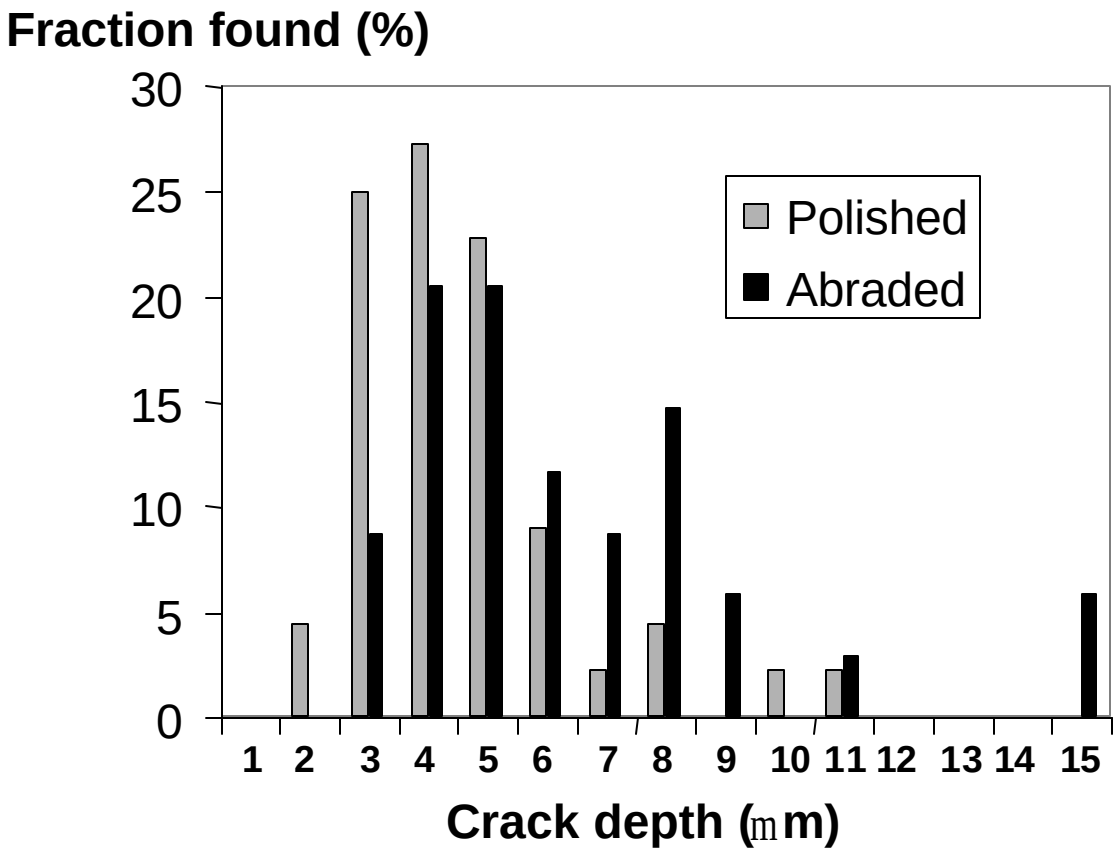

Figure 2: Surface quality in differently polished alumina specimens, as percentage of cracks found with 1μm size bands (i.e. "2μm" implies crack depth between 2 and 3μm). "Abraded" surface was ground with 600 grit SiC, "Polished" surface was ground with 600 grit SiC and then polished with 6μm diamond on a soft cloth until grinding marks we re removed. Results of Hertzian tests with alumina ball.

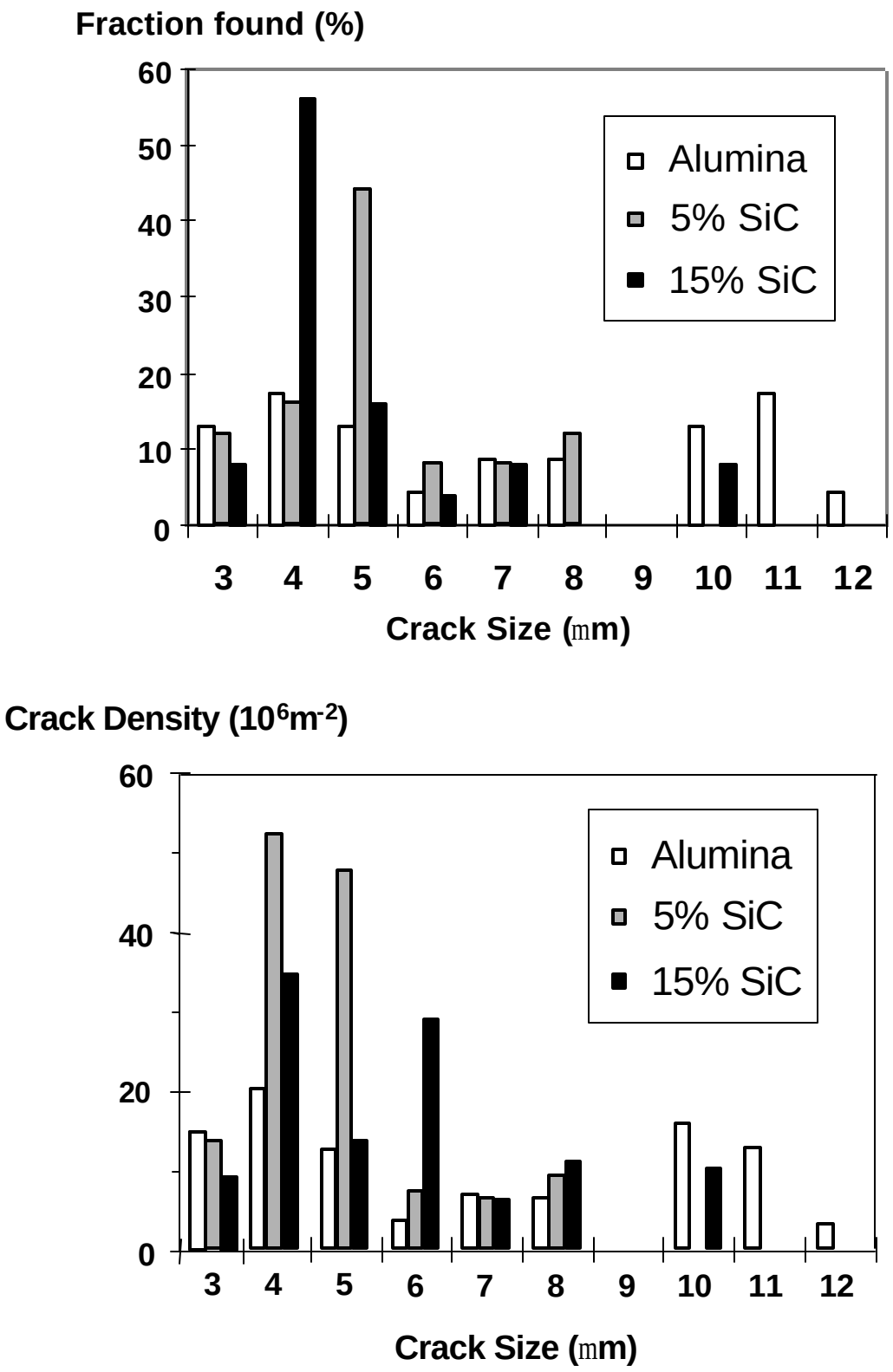

Figure 3: Hertzian tests for surface condition on Alumina / Sic "nanocomposites", all polished using the same treatment (6μm diamond powder finish). (a) number of cracks found in each 1μm size band; (b) the same data converted to area densities of cracks in each size band, using the "searched area" method.

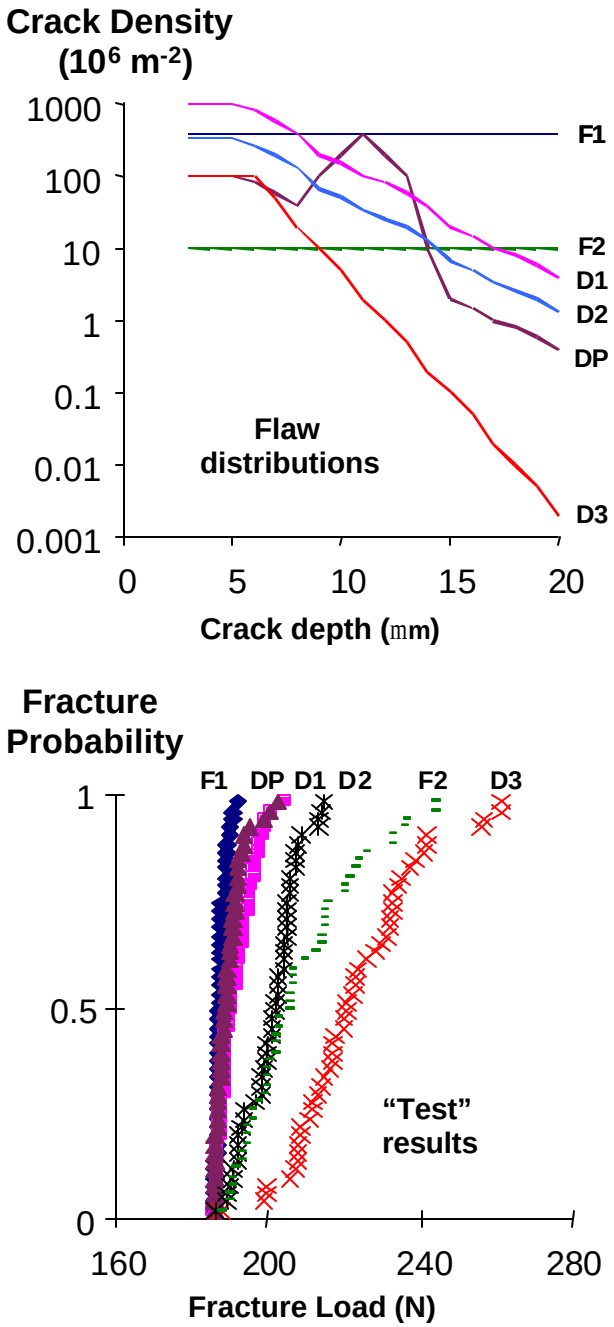

Figure 4: Simulations of Hertzian testing on alumina. The flaw distributions in Figure 4a were used in simulations of series of 50 tests with a 10mm diameter ball. Figure 4b shows the results, as probability of fracture as a function of indentation load.

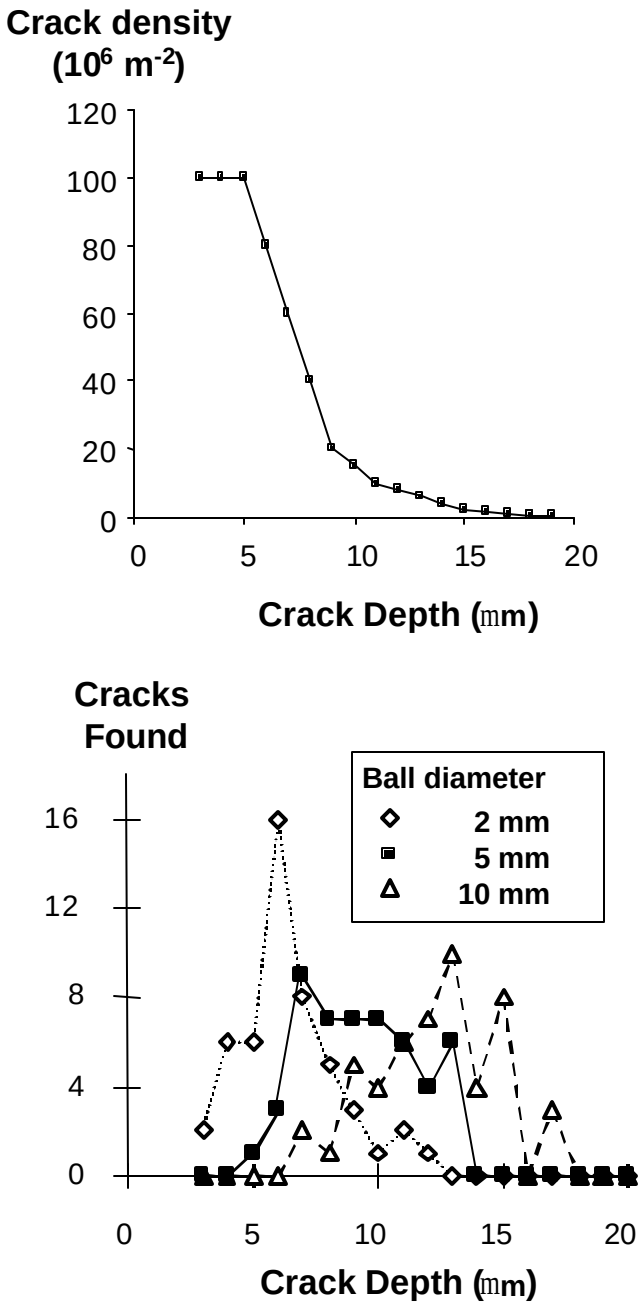

Figure 5: Simulations of Hertzian testing on alumina; effect of test ball size. The flaw distribution in Figure 5a was used in simulations of series of 50 tests with 2, 5 and 10mm diameter balls. Figure 5b shows the results, as number of cracks found of each size.

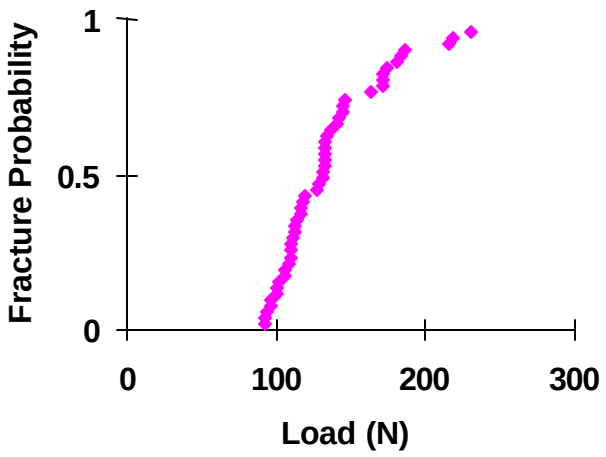

Figure 6: Typical experimental data for probability of fracture as a function of indentation load in glass. Note the well-defined minimum fracture load.

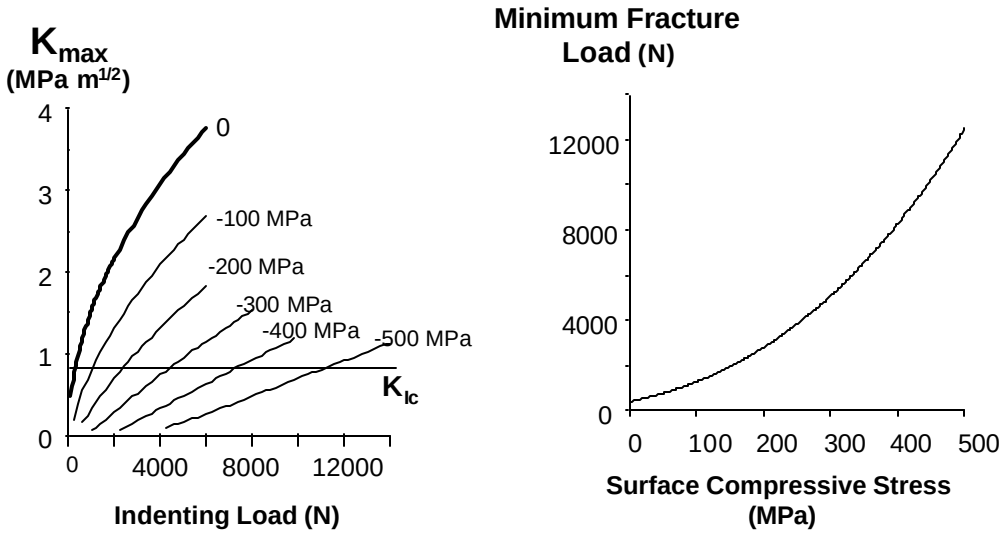

Figure 7: (a) Maximum stress intensity factor for any crack in the indented surface as a function of indentation load and surface stress; **(b)** minimum fracture load a function of surface stress. Calculations are for glass, indented with a 10mm diameter glass ball.

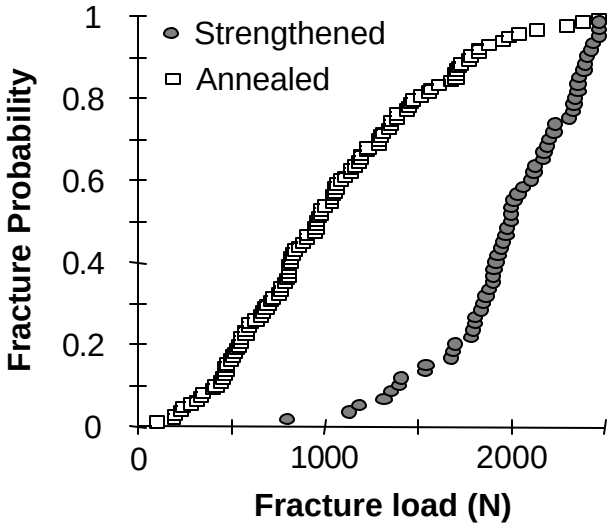

Figure 8: Cumulative probability of Hertzian fracture for annealed glass and for ion-strengthened glass. The threshold fracture load is much higher (800N) for the strengthened glass than for the annealed glass (89N).

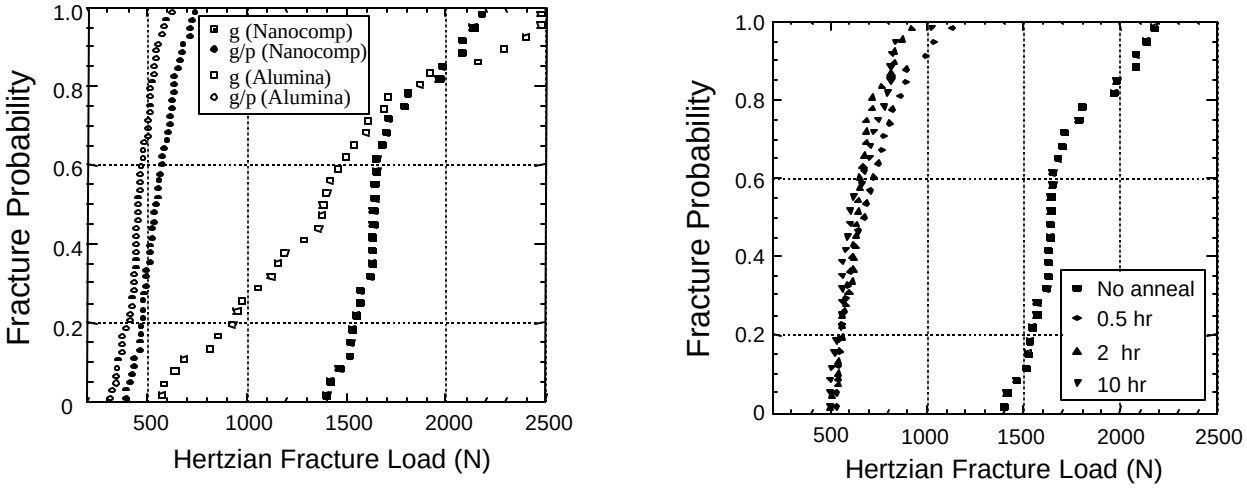

a) b)

Figure 9: Hertzian indentation fracture loads, shown as a cumulative probability of failure, from: (a) nanocomposite and equivalent grain size alumina specimens after grinding, g, and polishing, p; (b) nanocomposite specimens after grinding followed by annealing at 1250ºC for 0.5, 2 and 10 hours.

References

1 G.M. HAMILTON and L.E. GOODMAN: *Trans. Am. Soc. Metals*, 1966, **33**, 371-6.

2 T.R. WILSHAW: *J. Phys. D.,* 1971, **4**, 1567-81.

3 F.C. FRANK and B.R. LAWN: *Proc. R. Soc. Lond*., 1967, **A229**, 291-306.

4 R. WARREN: *Acta Metall.,* 1978, **26**, 1759-69.

5 R. MOUGINOT and D. MAUGIS: *J. Mater. Sci.,* 1985, **20,** 4354-76.

6 K. ZENG, K. BREDER, and D.J. ROWCLIFFE: *Acta metall. mater.,* 1992, **40**, 2595-600.

7 K. ZENG, K. BREDER, and D.J. ROWCLIFFE: *Acta metall. mater.,* 1992, **40**, 2601-05.

8 P.D. WARREN, D.A. HILLS and S.G. ROBERTS: *J. Mater Res.*, 1994, **9**, 3194-202.

9 D. NOWELL and D.A. HILLS: *J. Strain Anal*., 1987, **22**, 177-84.

10 S. LIN, P.D. WARREN and D.A. HILLS, *J. Euro. Ceram. Soc.,* 1998, **18**, 445-50.

11 W.E. SWINDLEHURST and B.R. LAWN, *J. Mater. Sci*., 1976, **11**, 1653-60.

12 P.D. WARREN, D.A. HILLS and S.G. ROBERTS: *J. Hard Materials*, 1994, **5**, 213-28.

13 C.C. ANYA and S.G. ROBERTS: *J. Euro. Ceram. Soc*., 1996, **16**, 1107-14.

14 P.D. WARREN: *J. Euro. Ceram Soc*, 1995, **15**, 201-7.

15 K.L. JOHNSON, J.J. O'CONNOR and A.C. WOODWARD: *Proc. R. Soc. London*, 1973, **A334**, 95.

16 G.R. ANSTIS, P. CHANTIKUL, B.R. LAWN and D.B. MARSHALL: *J. Am. Ceram. Soc*., 1981, **64**, 533-8.

17 C.B. PONTON and R.D. RAWLINGS: *Mat. Sci & Tech*., 1989, **5**, 865-72.

18 C.B. PONTON and R.D. RAWLINGS: *Mat. Sci & Tech*., 1989, **5**, 961-76.

19 F. AUERBACH, *Ann. Phys. Chem.*, 1891, **43**, 61.

20 B.R. LAWN: *J. Appl. Phys,* 1968, **39**, 4828-36.

21 S.G. ROBERTS, C.W. LAWRENCE, P.D. WARREN AND D.A. HILLS: *J. Am. Ceram. Soc*, in press.

22 J.M. BRADSHAW and B. TAYLOR: *The Physics of Non-Crystalline Materials*, eds L.D.. Pye, W.C. La Course and H.J Stevens., Taylor and Francis, London (1992), pp 471-475.

23 T. KISHII: *Optics and Lasers in Engineering*, 1983, **4**, 25-40.

24 K. NIIHARA: *J. Ceram. Soc. Jpn*., 1991, **99**, 974-82

---

25 L.C. STEARNS, J. ZHAO and M.P. HARMER: *J. Eur. Ceram. Soc.*, 1992, **10**, 473-77

26 J. ZHAO, L.C. STEARNS, M.P. HARMER, H.M. CHAN, G.A. MILLER and R.E. COOK: *J. Amer. Ceram. Soc*., 1993, **76**, 503-10.

27 C.E. BORSA, S. JIAO, R.I. TODD and R.J. BROOK: *J. Microscopy*, 1994, **177**, 305-12.

28 L.M. CARROLL, M. STERNITZKE and B. DERBY: *Acta Mater*., 1996, **44**, 4543-52.

29 H.Z. WU, C.W. LAWRENCE, S.G. ROBERTS and B. DERBY: *Acta Mater*., in press.